

# Quantitative Assessment of Motion Artifacts and Validation of a New Motion-Correction Program for Myocardial Perfusion SPECT

Naoya Matsumoto, Daniel S. Berman, Paul B. Kavanagh, James Gerlach, Sean W. Hayes, Howard C. Lewin, John D. Friedman, and Guido Germano

*Division of Nuclear Medicine, Department of Imaging; Division of Cardiology, Department of Medicine; and Artificial Intelligence in Medicine Program, Cedars-Sinai Medical Center, University of California Los Angeles School of Medicine, Los Angeles, California*

Patient motion during myocardial perfusion SPECT can produce images that show artifactual perfusion defects. The relationship between the degree of motion and the extent of artifactual perfusion defects is not clear for either single- or double-head detectors. Using both single- and double-head detectors and quantitative perfusion SPECT (QPS) software, we studied the pattern and extent of defects induced by simulated motion and validated a new automatic motion-correction program for myocardial perfusion SPECT. **Methods:** Vertical motion was simulated by upward shifting of the raw projection datasets in a returning pattern (bounce) and in a nonreturning pattern at 3 different phases of the SPECT acquisition (early, middle, and late), whereas upward creep was simulated by uniform shifting throughout the acquisition. Lateral motion was similarly simulated by left shifting of the raw projection datasets in a returning pattern and in a nonreturning pattern. Simulations were performed using single- and double-head detectors, and simulated motion was applied to projection images from 8 patients who had normal  $^{99m}\text{Tc}$ -sestamibi SPECT findings. Additionally, images from 130 patients with actual clinical motion were assessed before and after motion correction. The extent of perfusion defects was assessed by QPS, and a 20-segment, 5-point scoring system was used to assess the effect of motion on the presence and extent of perfusion defects. **Results:** Of 12 bounce simulations, the bouncing motion failed to produce significant ( $>3\%$ ) perfusion defects with either the single- or the double-head detector. With the single-head detector, early shifting created the largest defect, whereas with the double-head detector, shifting during the middle of the acquisition created the largest defect. With regard to upward creep, defects were of larger extent with the double- than the single-head detector. With the single-head detector, 8 of 20 simulated motion patterns yielded significant perfusion defects of the left ventricle, 7 (88%) of which were significantly improved after motion correction. With the double-head detector, 12 of 20 patterns yielded significant defects, all of which improved significantly after correction. Of 2,600 segments in the 130 patients

with actual clinical motion, only 1.3% (30/2,259) of segments that were considered normal (score = 0 or 1) changed to abnormal (score = 2–4) after motion correction, whereas 27% (92/341) of abnormal segments were reclassified as normal after motion correction. **Conclusion:** Artifactual perfusion defects created by simulated motion are a function of the time, degree, and type of motion and the number of camera detectors. Application of an automatic motion-correction algorithm effectively decreases motion artifacts on myocardial perfusion SPECT images.

**Key Words:** myocardial perfusion SPECT; motion correction; artifacts

**J Nucl Med 2001; 42:687–694**

**P**atient motion during myocardial perfusion SPECT acquisition is a well-recognized source of error in scan interpretation (1–4). The pattern and severity of motion-induced artifacts have been described for actual or simulated motion varying in type, timing, duration, magnitude, and direction during SPECT acquisition with single-head detectors (4–7). However, differences between motion artifacts produced with single-head detectors and motion artifacts produced with double-head detectors have not been investigated.

The best solution to patient motion is to prevent it during SPECT acquisition by, for example, using arm-holding devices or positioning the patient prone for imaging, the latter approach being also useful to reduce left ventricular inferior wall attenuation after acquisition (8). Motion artifacts can also be reduced after acquisition by manual shifting of individual projection images before reconstruction, although this process is time-consuming and subject to operator variability. Although several motion-correction programs are available to automatically or semiautomatically detect and compensate for motion in the projection datasets, none of these methods have proven robust or sufficiently practical to achieve wide clinical use (9–14). The goals of this study were, first, to investigate the relationship between

Received Dec. 1, 2000; revision accepted Mar. 16, 2001.

For correspondence or reprints contact: Guido Germano, PhD, Cedars-Sinai Medical Center, 8700 Beverly Blvd., Room A047 N, Los Angeles, CA 90048.

the degree of simulated motion and extent of artifactual perfusion defects for SPECT acquisitions with both single- and double-head detectors and, second, to determine the ability of a recently developed program to automatically correct simulated motion and clinical motion in a large cohort of patients.

## MATERIALS AND METHODS

Dual-isotope (rest  $^{201}\text{Tl}$ /postexercise  $^{99\text{m}}\text{Tc}$ -sestamibi) SPECT images were acquired on a gamma camera with a double-head detector in the  $90^\circ$  configuration (Vertex; ADAC Laboratories, Milpitas, CA) using a high-resolution, low-energy collimator; pseudocontinuous detector rotation (15); 64 projections over a  $180^\circ$  arc from  $+45^\circ$  right anterior oblique to  $-135^\circ$  left posterior oblique; and a noncircular orbit.  $^{201}\text{Tl}$  (111–167 MBq [3.0–4.5 mCi]) for rest images and  $^{99\text{m}}\text{Tc}$ -sestamibi (925–1,480 MBq [25–40 mCi]) for postexercise images were injected intravenously, with dose variation based on patient weight (16). Rest  $^{201}\text{Tl}$  images were acquired with a 30% window centered over the 68- to 80-keV photopeak and a 20% window over the 167-keV photopeak. Postexercise sestamibi acquisition used a 15% window over the 140-keV  $^{99\text{m}}\text{Tc}$  photopeak. The raw projection datasets were filtered with a Butterworth filter (for  $^{201}\text{Tl}$ : order, 10, and cutoff frequency, 0.5 cycle/pixel; for  $^{99\text{m}}\text{Tc}$ -sestamibi: order, 5, and cutoff frequency, 0.66 cycle/pixel; pixel size, 6.4 mm). No scatter or attenuation correction was applied. Filtered raw projection images were automatically reconstructed into transverse datasets. Then, the 3-dimensional location of the long axis of the left ventricle was determined automatically, and the short-, vertical long-, and horizontal long-axis images were generated (17,18).

Perfusion SPECT images were scored semiquantitatively using a 20-segment model for the left ventricle, including 6 segments in each of the distal, midventricular, and basal short-axis slices and 2 apical segments in a midventricular vertical long-axis slice (Fig. 1) (16). A 5-point scale for radiopharmaceutical uptake was used, in which 0 = normal uptake, 1 = mildly reduced uptake, 2 = moderately reduced uptake, 3 = severely reduced uptake, and 4 = no uptake. These scores were automatically derived using previously validated quantitative perfusion SPECT (QPS) software (Cedars-Sinai Medical Center, Los Angeles, CA). Automatically determined QPS scores have been previously shown to correlate strongly with expert visual scores (19). A measurement of the perfusion defect extent based on the percentage of pixels with counts below normal in the entire myocardium was also derived using QPS (19). As previously described, a threshold of 3% abnormal myocardial pixels was used for the detection of a significant perfusion defect by QPS. This relatively low threshold has

been shown to result in high sensitivity and specificity for detection of coronary artery disease (19).

## Simulated Motion

Eight patients (4 men, 4 women) who underwent dual-isotope rest  $^{201}\text{Tl}$ /postexercise gated  $^{99\text{m}}\text{Tc}$ -sestamibi myocardial perfusion SPECT were selected. The myocardial perfusion findings for these patients were completely normal by both visual and QPS analysis. The absence of motion was documented visually using cinematic display of the projection datasets, with motion estimated to be absent or less than 0.5 pixel in every patient (1 pixel = 6.4 mm). The number of myocardial counts as a function of the individual projection datasets was also measured, because the number was expected to vary with the amount of soft-tissue attenuation and the distance between camera and patient.

In the postexercise gated  $^{99\text{m}}\text{Tc}$ -sestamibi images, vertical motion was simulated by upward shifting of the raw projection datasets vertically in a returning (bounce) pattern and in a nonreturning pattern. Lateral motion was similarly simulated by left shifting of the raw projection datasets horizontally in a returning (bounce) pattern and in a nonreturning pattern, according to the formula  $D_i = dT \times \cos(\theta_i)$ , where  $D_i$  is the horizontal distance by which to shift image  $i$ ,  $dT$  is the amount of patient movement being simulated, and  $\theta_i$  is the angle between the camera and the patient for image  $i$ , with  $0^\circ$  corresponding to the anterior image (20).

Although all patient studies were acquired using a camera with a double-head detector, the data for the 8 patients with no motion and normal SPECT findings were used to simulate motion for acquisitions with both single- and double-head detectors. Because the total time required for acquisition with a double-head  $90^\circ$  detector is half that with a single-head detector for the same number of counts collected, the timing of simulated motion (shifting) was chosen on the basis of the detector type. For example, early shifting was timed at the 17th of 64 frames for one fourth of an acquisition with the single-head detector but only at the 9th of 64 frames in an acquisition with the double-head detector (frames 1–32 and 33–64 were acquired simultaneously in the latter). One-, 2-, and 3-pixel bounce (returning motion) was simulated by moving 3 consecutive frames (17–19 in a 64-frame acquisition with the single-head detector; 17–19 and 49–51 in a 64-frame acquisition with the double-head detector).

Both nonreturning shifting motion and upward creep (4) were simulated for acquisitions with single- and double-head detectors. For the single-head detector, all combinations of motion by 1, 2, and 3 pixels in the vertical or lateral direction were applied during the early (frames 17–64), middle (frames 33–64), and late (frames 49–64) phases of the acquisition. For the double-head detector, the

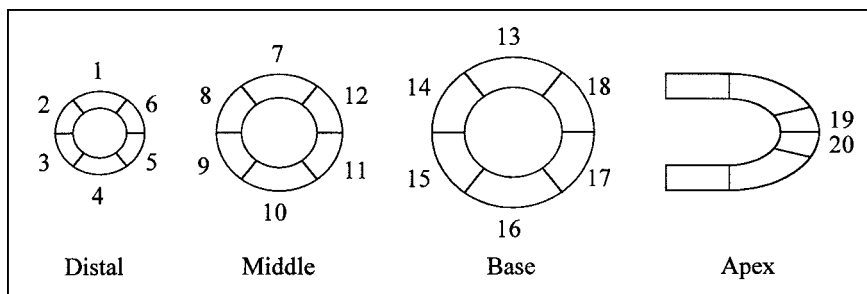


**FIGURE 1.** Cedars-Sinai 20-segment model.

same combinations were applied during the early (frames 9–32 and 41–64), middle (frames 17–32 and 49–64), and late (frames 25–32 and 57–64) phases of the acquisition. Uniform upward creep totaling 2 or 3 pixels was applied to all 64 frames consecutively (Fig. 2).

Twelve different types of bounce were simulated for acquisitions with single- and double-head detectors, involving 2 directions (vertical and lateral) and 3 amounts (1, 2, and 3 pixels). Eighteen different types of nonreturning motion were simulated for acquisitions with either the single- or the double-head detector, involving 2 directions (vertical and lateral), 3 timings (early, middle, and late), and 3 amounts (1, 2, and 3 pixels). Adding upward creep (2 or 3 pixels) brought the total to 26 simulated motion patterns for acquisitions with the single-head detector and 26 for acquisitions with the double-head detector.

### Nonsimulated Clinical Motion

One hundred thirty consecutive patients (100 men [77%; mean age,  $66 \pm 11.8$  y], 30 women [23%; mean age,  $66 \pm 11.6$  y]) whose scans were considered to show actual motion were selected from our clinical patient population imaged on the Vertex camera. The distribution of naturally occurring motion in this population was as follows: 63% vertical motion (of these, 78% represented multiple bounce and 22% single bounce), 26% upward creep, 7% vertical and horizontal motion, and 4% horizontal motion.

### Evaluation of Motion Artifacts and Motion-Correction Program

*Simulated Motion.* After the raw projection images of the scans with normal findings were moved to simulate motion, the motion-corrupted images were reconstructed automatically. The motion-correction program was applied to the motion-corrupted projection images, generating motion-corrected images that were then reconstructed automatically using the same reconstruction limits and reorientation axes (21) and analyzed with QPS.

*Actual Clinical Motion.* In patients whose scans showed actual clinical motion, the extent of motion seen on the raw projection

images was visually classified into 4 categories (1, 2, 3, and 4 pixels). Perfusion SPECT images were automatically scored using QPS, with abnormal perfusion being defined as a score  $\geq 2$  (16,19,22). The motion-correction program was then applied to all cases of actual clinical motion, and the effect of the program on motion and motion artifacts was evaluated visually on the projection images and quantitatively on the reconstructed SPECT slices using QPS. In total, 2,600 segments (20 segments for 130 clinical patients) were scored before and after application of the motion-correction program.

### Motion-Correction Algorithm

Our motion-correction algorithm (23) is a simple extension of the projection–reprojection technique already described for sinogram data (24). The algorithm compensates for motion in an acquired SPECT dataset by computing, for each projection, the displacement vector that maximizes agreement between the projection and its corresponding reprojection, which is generated from the transverse reconstruction. This agreement is expressed by a cost function of the original projection, corresponding reprojection, and vector displacement that is designed to return a maximal value when corresponding features in the original projection and displaced reprojection are in closest proximity. In essence, the cost function is computed by matching gradients in the projection and reprojection, with additional weight given to regions corresponding to the myocardium (or other organ to be motion corrected) in the transverse reconstruction image. The motion-corrected dataset is then generated by translating each projection in the acquired dataset by its corresponding displacement vector.

### Statistical Analysis

Data before and after motion correction were compared using the paired *t* test.  $P < 0.05$  was considered statistically significant. Agreement of perfusion scores before and after correction in cases of clinical motion was assessed by unweighted  $\kappa$  and SE statistics.

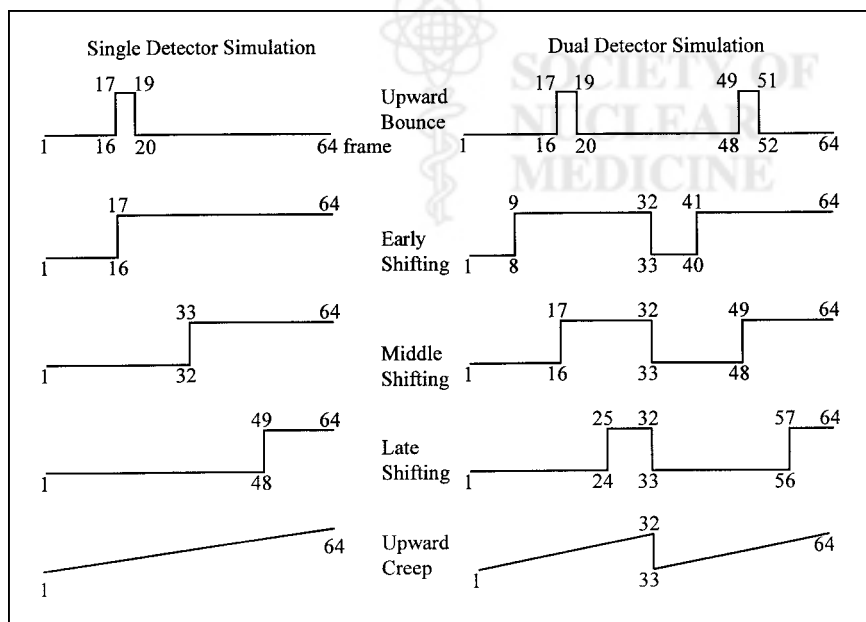


**FIGURE 2.** Upward bounce, vertical upward shifting, and upward creep simulations imaged with single- and double-head detectors. Lateral bounce and shifting (not shown) were simulated by left bounce and shifting, with timing same as for vertical motion.

## RESULTS

### Pattern and Extent of Simulated Perfusion Defects

Bouncing motion (vertical or lateral) failed to produce significant (>3%) perfusion defects: the average defects for 1-, 2-, and 3-pixel shifting were 0.2%, 0.6%, and 0.9%, respectively. In all simulations of vertical and lateral motion for acquisitions with the single- and double-head detectors, 1-pixel shifting did not create a significant perfusion defect. Three-pixel shifting usually produced severe perfusion defects and obvious distortion of ventricular shape, sometimes resulting in images not amenable to quantitative analysis. Two-pixel shifting was deemed most suitable for evaluating the extent and pattern of perfusion defects. Defect values are shown as mean  $\pm$  SD.

With 2-pixel upward nonreturning motion and acquisition using the double-head detector, shifting during the middle phase created the largest defect (13.5%  $\pm$  7.0%), followed by late shifting (5.9%  $\pm$  4.9%) and early shifting (3.1%  $\pm$  2.2%). With the same type of motion but acquisition with the single-head detector, early shifting resulted in the largest defect (9.8%  $\pm$  5.2%), followed by shifting during the middle phase (6.9%  $\pm$  3.8%) and late shifting (0.3%  $\pm$  0.5%).

With 2-pixel lateral nonreturning motion and acquisition using either the single- or the double-head detector, the trend in defect extent was the same as with upward shifting. Specifically, for the double-head detector, defects of 5.1%  $\pm$  3.6%, 3.9%  $\pm$  3.3%, and 2.5%  $\pm$  2.1% occurred with shifting during the middle, late, and early phases, respectively, whereas for the single-head detector, defects of 4.3%  $\pm$  4.8%, 1.4%  $\pm$  1.3%, and 0.1%  $\pm$  0.4% occurred with shifting during the early, middle, and late phases, respectively.

The extent of defects produced by 2-pixel upward creep was 1.1%  $\pm$  2.7% for the single-head detector and 2.0%  $\pm$  2.8% for the double-head detector. Three-pixel upward creep resulted in defects of 3.3%  $\pm$  1.9% for the single-head detector and 6.9%  $\pm$  5.7% for the double-head detector.

### Myocardial Count Distribution

The average myocardial counts as a percentage of the total counts in the projection images were 12.2% (frames 1–8), 14.6% (frames 9–16), 14% (frames 17–24), 12.7% (frames 25–32), 12% (frames 33–40), 11.9% (frames 41–48), 11.8% (frames 49–56), and 10.8% (frames 57–64). As expected, maximal myocardial counts were seen in the

frames in which the detector was in the anterior position (frames 9–24).

### Defect Extent Before and After Correction of Simulated Motion

**Bounce.** In our 12 bounce simulations, motion artifacts did not create significant perfusion defects. Visual evaluation of the cinematic raw projection datasets before and after motion correction showed that all the simulated vertical and lateral bounces were completely corrected by the motion-correction program.

**Shifting and Upward Creep.** For the single-head detector, of the 14 cases of simulated motion involving 2- or 3-pixel upward shifting and upward creep, 8 cases yielded significant defects, 7 of which (88%) were significantly improved after motion correction. The average extent of defects improved from 7.0%  $\pm$  2.2% before correction to 1.6%  $\pm$  0.6% after correction for 2-pixel shifting and from 10%  $\pm$  6.2% before correction to 4.0%  $\pm$  3.0% after correction for 3-pixel shifting (Figs. 3 and 4).

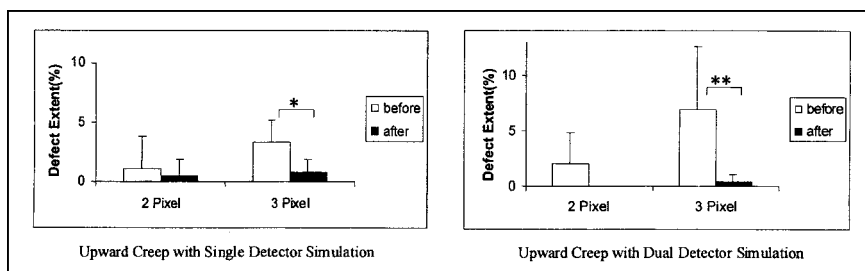
For the double-head detector, 12 of 14 cases (86%) of simulated motion yielded significant defects, 12 of which (100%) improved significantly after correction. Specifically, the average extent of defects decreased from 6.3%  $\pm$  3.7% before correction to 0.8%  $\pm$  0.7% after correction for 2-pixel shifting and from 11.1%  $\pm$  5.2% before correction to 2.7%  $\pm$  2.7% after correction for 3-pixel shifting (Figs. 3 and 5).

### Correction of Clinical Motion

Of the 130 patients with actual clinical motion, motion on the raw projections was judged to be 4-pixel in 2%, 3-pixel in 11%, 2-pixel in 52%, and 1-pixel in 35% before correction. After correction, no patient showed 3- or 4-pixel deviation, and 2-pixel deviation occurred in 2% of patients. The remaining patients had 0- or 1-pixel deviation. In no case did motion worsen after correction.

Segment scores automatically determined by QPS before and after motion correction are shown in Table 1. Only 1.3% (30/2,259) of segments that were considered normal (score = 0 or 1) changed to abnormal (score = 2–4) after motion correction, whereas 27% (92/341) of abnormal segments were reclassified as normal after motion correction. Figure 6 illustrates a patient for whom motion correction changed the quantitative summed stress score (SSS) from 4 (mildly abnormal) to 1 (normal) and the quantitative defect extent from 4% to 1%.

**FIGURE 3.** Defect extent before and after motion correction for upward creep simulation imaged with single- and double-head detectors. \* $P < 0.05$ ; \*\* $P < 0.01$ .





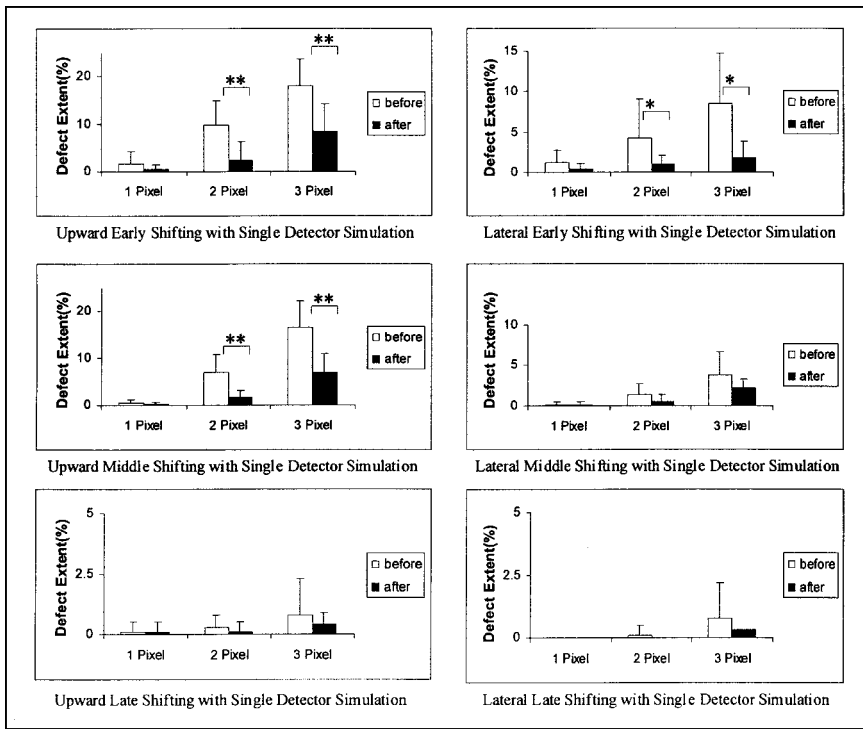


**FIGURE 4.** Defect extent before and after motion correction for upward and lateral shifting simulations imaged with single-head detector. \* $P < 0.05$ ; \*\* $P < 0.01$ .

## DISCUSSION

Despite multiple advances in the technology of myocardial perfusion SPECT, patient motion remains a problematic source of error. This article describes the validation of an automatic motion-correction program. For simulated motion, our findings showed that 1-pixel motion usually does

not produce perfusion artifacts and that perfusion defects are common with greater degrees of motion. The motion-correction program significantly eliminated artifactual defects in nearly all motion simulations. Furthermore, in the large group of patients showing actual clinical motion, application of the motion-correction program markedly re-

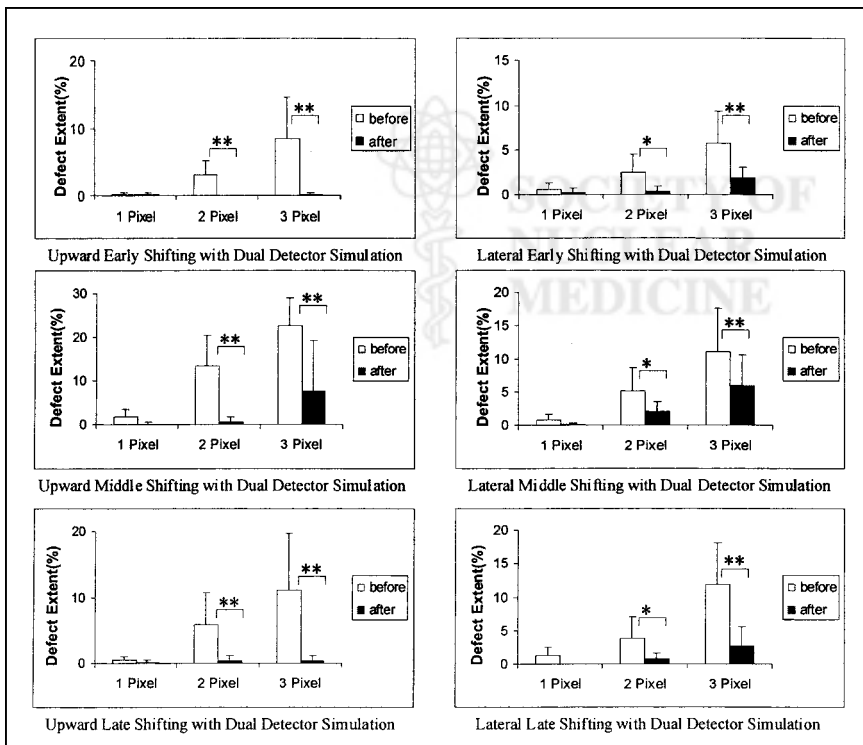


**FIGURE 5.** Defect extent before and after motion correction for upward and lateral shifting simulations imaged with double-head-detector. \* $P < 0.05$ ; \*\* $P < 0.01$ .

**TABLE 1**  
Segmental Distribution Before and After Motion Correction: 2,600 Segments for 130 Patients

QPS perfusion scores after motion correction	QPS perfusion scores before motion correction				
	0	1	2	3	4
0	1,802	152	33	0	0
1	33	242	46	13	0
2	6	22	108	19	2
3	0	2	3	68	7
4	0	0	0	1	41

Agreement = 87%; unweighted  $\kappa$  = 0.70; SE = 0.014.

duced the extent of apparent perfusion defects and rarely was associated with creation of new perfusion defects.

Predictably, the effect of patient motion in producing artifactual perfusion defects was found to depend on the amount of motion. In our studies involving simulated motion, the average defect extent corresponding to 1-pixel shifting (6.4 mm) was <1% of the left ventricle (0.6% and 0.8% for the single- and double-head detectors, respectively). Thus, motion of up to 1 pixel did not create a significant perfusion defect and would not be expected to affect quantitative SPECT interpretation. The average defect extent corresponding to 2-pixel shifting was significant (3.8% and 5.7% for the single- and double-head detectors, respectively). With 3-pixel shifting, the average was 8.1% and 11.8% for the single- and double-head detectors, respectively (Figs. 4 and 5). Regarding simulation of upward creep, the average defect extent associated with the single-head detector was 1.1% for 2-pixel creep and 3.3% for 3-pixel creep,

whereas that with the double-head detector was 2.0% for 2-pixel creep and 6.9% for 3-pixel creep.

A common assumption is that motion artifacts affect acquisitions with double-head detectors more than acquisitions with single-head detectors. This assumption is related to the fact that a single occurrence of nonreturning motion with a double-head detector will affect twice as many projections as with a single-head detector and that the greatest amount of motion is seen between the first frame of the second detector and the last frame from the first detector, corresponding to a point with relatively high myocardial counting rates. On the other hand, acquisitions with single-head detectors are twice as long as with double-head detectors for the same number of collected counts, and therefore, the chance that the patient will move during acquisitions with single-head detectors is greater (25). The average extent of perfusion defects produced by simulated motion in this study supports the hypothesis that acquisitions with double-head detectors are more vulnerable to motion.

The results of this study also showed that defect extent has a strong relationship with the timing of shifting. In fact, early upward shifting created a larger defect (9.8%) in simulations using the single-head detector than in those using the double-head detector (3.1%), but upward shifting during the middle of the acquisition created a smaller defect with the single-head detector than with the double-head detector (6.9% vs. 13.5%, respectively). In acquisitions with both the single- and the double-head detectors, frame 17 corresponds to the anterior projection, in which the left ventricular myocardium has maximal counts. The larger perfusion artifact found with early shifting in simulations with the single-head detector is, at least in part, likely related to count distribution. As a general rule, motion in the

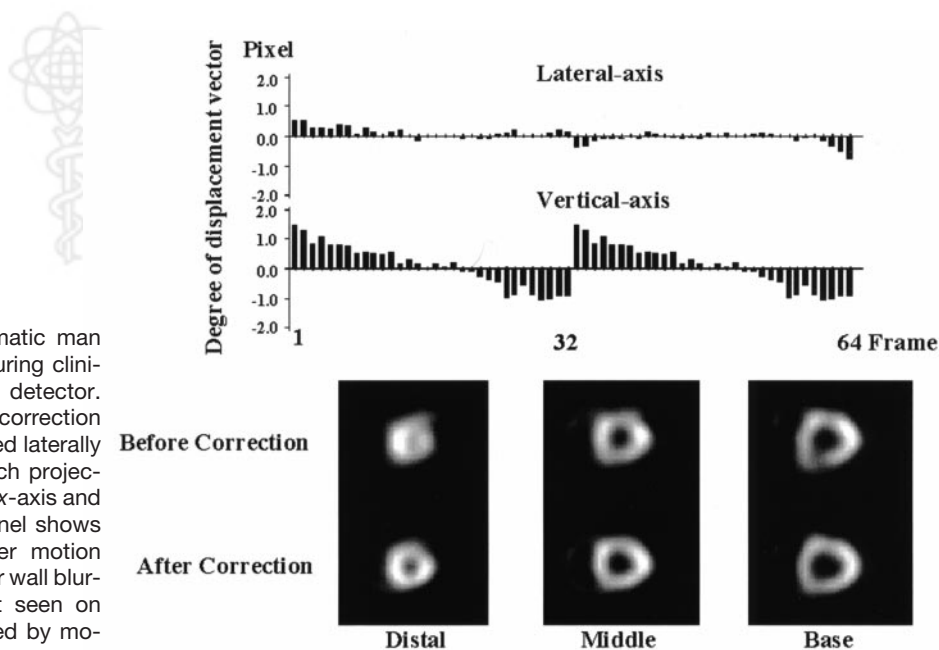


**FIGURE 6.** A 62-y-old asymptomatic man who had 2.5-pixel upward creep during clinical acquisition with double-head detector. Top panel shows extent of motion correction automatically determined and applied laterally (x-axis) and vertically (y-axis) to each projection image. Motion was slight along x-axis and significant along y-axis. Bottom panel shows short-axis images before and after motion correction. Middle and distal anterior wall blurring and basal inferior wall defect seen on uncorrected images were diminished by motion correction.

projections in which myocardial counts are greater appears to cause larger motion artifacts. With the double-head-detector simulation, shifting during the middle of the acquisition created the greatest defect, consistent with its occurrence at the frame that had maximal counts. Early and late shifting involved the same number of misaligned frames and might have been expected to result in similar outcomes, but in our study late shifting was found to affect defect extent more than did early shifting. This phenomenon is once again related to the relative difference in myocardial counts at the points where the shifting occurred.

With lateral shifting, the influence of motion is more complex, because the effect of shifting is greatest in the anterior image (where motion is parallel to the detector) and least in the lateral image (where motion is perpendicular to the detector) (20). Thus, although vertical motion will affect projection images similarly throughout the angles of acquisition, lateral motion will have a varying effect on the projection images. In a simulated motion study with a single-head detector, Cooper et al. (20) reported that early lateral shifting created a larger defect than did shifting during the middle or late phases of the acquisition (similarly to our findings), but upward shifting during the middle phase created a larger defect than did early shifting. This latter finding is different from our findings, possibly because of a difference in the shifting technique (integral vs. fractional pixel moves), the use of an active rather than a low-pass filter, or the use of a different quantitative perfusion algorithm (26). With regard to upward creep, the defect extent was more extensive in motion simulations using the double-head detector than in those using the single-head detector.

We conclude that motion-induced perfusion defects are affected by the type and amount of motion, motion timing, and number of camera detectors.

With respect to the correction of simulated motion, bounce simulations resulted in artifactual perfusion defects whose extent was not significant with either the single- or the double-head detector. Therefore, the quantitative difference in the extent of defects before and after motion correction was not a suitable criterion for evaluation of the motion-correction program. Visual evaluation of the cinematic projections before and after correction for bounce showed that the motion-correction program eliminated the appearance of bounce. In simulations with the single-head detector, the extent of perfusion defects created by 2-pixel shifting and creep was successfully improved by the automatic motion-correction algorithm (7.0%–1.6%). With 3-pixel shifting, the extent of defects was significantly decreased but the average extent after correction was still abnormal (10%–4.0%). In simulations with the double-head detector, the extent of perfusion defects created by 2- and 3-pixel shifting and creep was lessened after motion correction (from 6.3% to 0.8% for 2-pixel shifting and from 11.1% to 2.7% for 3-pixel shifting). On the basis of these findings,

we recommend that clinical studies with >2-pixel motion be repeated rather than corrected for motion.

Published motion-correction algorithms include cross-correlation, diverging squares, and 2-dimensional fit approaches based on the comparison of adjacent raw projection datasets (9–12). The cross-correlation algorithm uses the entire y-axis myocardial count profile and is potentially sensitive to extracardiac uptake. The diverging squares algorithm, in its published implementation, requires manual outlining of the myocardium; this algorithm is not affected by extracardiac uptake but is sensitive to overlapping uptake. The 2-dimensional fit algorithm also requires manual positioning of a region of interest around the heart in the 45° left anterior oblique projection but is not affected by extracardiac uptake (12). The motion-correction algorithm investigated in the current study is completely automatic and not affected by extracardiac uptake. Overlapping extracardiac uptake may still hamper motion correction by preventing automatic identification and segmentation of the myocardium. However, simply constraining the algorithm to operate within a manually positioned ellipse containing the myocardium usually preserves the ability of the algorithm to automatically determine and apply motion-correction offsets to all projections.

With respect to actual clinical motion, several studies have evaluated the effectiveness of correction techniques by analyzing improvements in projection data (9–12). Other investigators have used quantitative analysis applied to <sup>201</sup>Tl SPECT (14,20,26). We used both visual scoring of projection images before and after motion correction and application of a quantitative program to the evaluation of motion artifacts on <sup>99m</sup>Tc-sestamibi SPECT images. Evaluating the extent of perfusion defects using QPS complements review of the projection data, because motion does not necessarily create clinically significant defects. In our study, motion correction changed 27% (92/341) of abnormal segments (score = 2–4) to normal (specifically, 33 segments from 2 to 0, 46 segments from 2 to 1, and 13 segments from 3 to 1). This finding supports the suggestion that motion correction leads to a decreased SSS and could thus be important to the accuracy of prognostic assessments (27). Only 1.3% (30/2,259) of normal segments (score = 0 or 1) were changed to abnormal (score = 2–4) by motion correction. The 130 clinical patients in whom motion occurred were not all healthy. Of the 1.3% of segments that were classified as abnormal after motion correction, many may reflect the presence of true perfusion defects. Thirty segments in 25 patients whose findings appeared normal before motion correction showed perfusion defects after motion correction. Ten of these 25 patients underwent coronary angiography within 3 mo of the SPECT study. In 9 patients, the perfusion defects seen only on the motion-corrected studies corresponded to territories supplied by coronary arteries with >50% stenoses. Although the angiographic correlations were present in only 9 of 25 patients, these findings suggest that motion correction does not create artifactual

defects. In some cases in which perfusion defects were more marked after motion correction, the motion-correction program improved left ventricular shape dramatically.

Finally, our study was limited in that it investigated motion artifacts using a frame-shifting simulation technique in which the heart was moved between projections. Clinical motion will likely occur during acquisition of a given projection, therefore resulting in blurring of that projection and misalignment with successive projections. Our motion-correction method corrected only the net motion occurring in any projection, without attempting recovery within the projection. Moreover, the algorithm corrected only heart motion along the  $x$ - and  $y$ -axes, not heart torsion around the long axis.

In the 130 clinical patients, the automatic motion-correction program occasionally could not locate the heart. The success rate of the algorithm was described to be >90% with reference to myocardial segmentation from projection images in automatic reconstruction and reorientation (21). In those patients in whom the algorithm fails to identify the myocardium, the algorithm can be constrained to operate within an elliptic region of interest containing the myocardium, ensuring segmentation.

## CONCLUSION

The current study analyzed the pattern and extent of perfusion defects produced by simulated motion in acquisitions with both single- and double-head detectors. Our newly developed motion-correction program successfully compensated for both simulated and clinical moderate motion, working well with both single- and double-head detectors and improving SPECT interpretation.

## ACKNOWLEDGMENT

Cedars-Sinai Medical Center receives royalties from the licensing of QPS and the motion-correction algorithm described in this article. A minority portion of these royalties is shared by the algorithm developers. This study was presented in part at the annual meeting of the Society of Nuclear Medicine, St. Louis, MO, June 2000.

## REFERENCES

1. Friedman J, Berman DS, Van Train K, et al. Patient motion in thallium-201 myocardial SPECT imaging: an easily identified frequent source of artifactual defect. *Clin Nucl Med*. 1988;13:321–324.
2. DePuey EG, Garcia EV. Optimal specificity of thallium-201 SPECT through recognition of imaging artifacts. *J Nucl Med*. 1989;30:441–449.
3. DePuey E. Artifacts clarified by and caused by gated myocardial perfusion SPECT. In: Germano G, Berman D, eds. *Clinical Gated Cardiac SPECT*. Armonk, NY: Futura Publishing; 1999:183–237.
4. Friedman J, Van Train K, Maddahi J, et al. “Upward creep” of the heart: a frequent source of false-positive reversible defects during thallium-201 stress-redistribution SPECT. *J Nucl Med*. 1989;30:1718–1722.
5. Sorrell V, Figueroa B, Hansen CL. The “hurricane sign”: evidence of patient motion artifact on cardiac single-photon emission computed tomographic imaging. *J Nucl Cardiol*. 1996;3:86–88.
6. Botvinick EH, Zhu YY, O’Connell WJ, Dae MW. A quantitative assessment of patient motion and its effect on myocardial perfusion SPECT images. *J Nucl Med*. 1993;34:303–310.
7. Prigent FM, Hyun M, Berman DS, Rozanski A. Effect of motion on thallium-201 SPECT studies: a simulation and clinical study. *J Nucl Med*. 1993;34:1845–1850.
8. Kiat H, Van Train KF, Friedman JD, et al. Quantitative stress-redistribution thallium-201 SPECT using prone imaging: methodologic development and validation. *J Nucl Med*. 1992;33:1509–1515.
9. Eisner RL, Noever T, Nowak D, et al. Use of cross-correlation function to detect patient motion during SPECT imaging. *J Nucl Med*. 1987;28:97–101.
10. Cooper JA, Neumann PH, McCandless BK. Detection of patient motion during tomographic myocardial perfusion imaging. *J Nucl Med*. 1993;34:1341–1348.
11. Geckle WJ, Frank TL, Links JM, Becker LC. Correction for patient and organ movement in SPECT: application to exercise thallium-201 cardiac imaging. *J Nucl Med*. 1988;29:441–450.
12. O’Connor MK, Kanal KM, Gebhard MW, Rossman PJ. Comparison of four motion correction techniques in SPECT imaging of the heart: a cardiac phantom study. *J Nucl Med*. 1998;39:2027–2034.
13. Germano G, Chua T, Kavanagh PB, Kiat H, Berman DS. Detection and correction of patient motion in dynamic and static myocardial SPECT using a multi-detector camera. *J Nucl Med*. 1993;34:1349–1355.
14. Leslie WD, Dupont JO, McDonald D, Peterdy AE. Comparison of motion correction algorithms for cardiac SPECT. *J Nucl Med*. 1997;38:785–790.
15. Germano G, Van Train K, Kiat H, Berman D. Digital techniques for the acquisition, processing, and analysis of nuclear cardiology images. In: Sandler MP, ed. *Diagnostic Nuclear Medicine*. 3rd ed. Baltimore, MD: Williams and Wilkins; 1995:347–386.
16. Berman DS, Kiat H, Friedman JD, et al. Separate acquisition rest thallium-201/stress technetium-99m sestamibi dual-isotope myocardial perfusion single-photon emission computed tomography: a clinical validation study. *J Am Coll Cardiol*. 1993;22:1455–1464.
17. Germano G, Berman D. Acquisition and processing for gated perfusion SPECT: technical aspects. In: Germano G, Berman D, eds. *Clinical Gated Cardiac SPECT*. Armonk, NY: Futura Publishing; 1999:93–113.
18. Germano G, Kavanagh PB, Su HT, et al. Automatic reorientation of three-dimensional, transaxial myocardial perfusion SPECT images. *J Nucl Med*. 1995; 36:1107–1114.
19. Sharir T, Germano G, Waechter P, et al. A new algorithm for the quantitation of myocardial perfusion SPECT. I. Validation and diagnostic yield. *J Nucl Med*. 2000;41:720–727.
20. Cooper JA, Neumann PH, McCandless BK. Effect of patient motion on tomographic myocardial perfusion imaging. *J Nucl Med*. 1992;33:1566–1571.
21. Germano G, Kavanagh PB, Chen J, et al. Operator-less processing of myocardial perfusion SPECT studies. *J Nucl Med*. 1995;36:2127–2132.
22. Germano G, Kavanagh P, Waechter P, et al. A new algorithm for the quantitation of myocardial perfusion SPECT. I. Technical principles and reproducibility. *J Nucl Med*. 2000;41:712–719.
23. Matsumoto N, Berman DS, Kavanagh PB, et al. Quantitative validation of a new patient motion correction program for myocardial perfusion SPECT [abstract]. *J Nucl Med*. 2000;41(suppl):45P–46P.
24. Huang SC, Yu DC. Capability evaluation of a sinogram error detection and correction method in computed tomography. *IEEE Trans Nucl Sci*. 1992;39: 1106–1110.
25. Hillier D, Wallis J. Myocardial SPECT motion artifact as a function of motion type and number of camera detectors [abstract]. *J Nucl Med*. 1999;40(suppl): 126P.
26. Eisner R, Churchwell A, Noever T, et al. Quantitative analysis of the tomographic thallium-201 myocardial bullseye display: critical role of correcting for patient motion. *J Nucl Med*. 1988;29:91–97.
27. Hachamovitch R, Berman DS, Shaw LJ, et al. Incremental prognostic value of myocardial perfusion single photon emission computed tomography for the prediction of cardiac death: differential stratification for risk of cardiac death and myocardial infarction. *Circulation*. 1998;97:535–543.